POAC'15
Trondheim, Norway

Proceedings of the 23rd International Conference on
Port and Ocean Engineering under Arctic Conditions
June 14-18, 2015
Trondheim, Norway

SIMULATIONS OF ICE RUBBLING AGAINST CONICAL STRUCTURES USING 3D DEM

David Morgan [1], Robert Sarracino [1], Richard McKenna [1,2], Jan W. Thijssen [3]

[1]C-CORE Centre for Arctic Resource Development (CARD), St. John's, NL, Canada

[2] R.F. McKenna Associates, Wakefield, QC, Canada

[3] C-CORE, St. John's, NL, Canada

ABSTRACT

Understanding ice rubble build-up is important in designing structures such as offshore platforms, bridge supports, and breakwaters for use in arctic and cold regions. Past numerical investigations to understand rubble pile formation and ice loads against slopes in two dimensions indicate that ice thickness and structure slope angle are dominant parameters.

This work uses a three-dimensional discrete element method (3D DEM) bonded particle model to simulate ice interacting with an upward-sloping cone. As with past 2D work on slopes, this investigation considered ice thickness and slope angle, but also considered block/particle size and sheet composition. Rubble pile characteristics of interest included height, shape, volume, and formation mechanisms (such as sliding, rotation, and collapse). In extending the 2D slope to a 3D cone, the geometry of the Confederation Bridge across Canada's Northumberland Strait was used a starting point.

This paper focuses on qualitative observations and learnings arising from the 3D simulations. These insights contribute to our current understanding of ice interaction with cones and serve to guide others wishing to undertake similar 3D DEM research into ice. The paper concludes with a discussion of potential future extensions, such as the use of finely-tuned DEM models and parameters to more accurately estimate ice loads against conical structures, and the repetition of similar numerical experiments to include ridges.

INTRODUCTION

Understanding sea ice rubble build-up is important in designing structures such as offshore platforms, bridge supports, and breakwaters for use in arctic and cold regions. Much research has been undertaken to understand rubbling on sloped structures through field observation (e.g., Brown et al. (2010)) and model tests (e.g., Lu et al. (2014)). Similarly, there are a number of analytical approaches to this problem which have been developed to calculate extreme loads (e.g., ISO 19906:2010). As well, ice rubbling on slopes has been simulated using numerical methods (e.g., Paavilainen and Tuhkuri (2013)).

This paper focuses on qualitative observations and learnings arising from three-dimensional discrete element method (3D DEM) simulations of an ice sheet hitting an upward-sloping cone to observe rubble pile formation and clearance around the sides. In contrast with past 2D investigations of ice interactions with slopes, which use finite element methods (FEM) to determine ice sheet fracture, this investigation used a bonded particle model developed for the LIGGGHTS DEM code (see Kloss et al. (2012)) to realize fracture solely using DEM.

The discrete element method was initially developed by Cundall (1971) in the context of rock mechanics. The method has since been used in a variety of domains, most notably in those involving granular materials (e.g., pharmaceutical mixing, agricultural grains, crushed ore) and brittle solids (e.g., rock, ice). Early use of DEM to model ice can be seen in the works of Hopkins, Hibler, and Flato (Hopkins and Hibler (1991a, 1991b); Hopkins et al. (1991)) in which each block of unbreakable ice rubble is represented by a DEM particle. DEM has also been used to model ice at larger scales: for example, Richard and McKenna (2013) represent each unbroken ice floe as a particle.

Examples of the use of 3D DEM in ice research are few. Most investigations into rubbling on slopes using DEM have been in two dimensions (e.g., Paavilainen and Tuhkuri (2012, 2013)), which serves well to represent a "wide" sloping structure, such as a caisson wall, shoreline, or breakwater. Work by Haase et al. (2010) considers the problem in 3D by using unbonded polygonal blocks of unconsolidated ice rubble to represent a ridge and keel striking the conical base of a pier of the Confederation Bridge across Canada's Northumberland Strait. Other 3D DEM work is limited to that of Lubbad and Løset (2011), Metrikin and Løset (2013), Metrikin et al. (2012a, 2012b), and Vroegrijk (2012) on ship-ice interaction, Kioka et al. (2010) on interactions with piles, and Sorsimo and Heinonen (2014), Polojärvi and Tuhkuri (2014, 2013, 2009), and Polojärvi et al. (2012) on punch-through experiments.[1]

Insights gained from the simulations featured in this work are useful in supporting and/or contrasting our current understanding of ice interaction with sloping structures (which has been arrived at through observation, model tests, analytical methods, and 2D simulations), and in guiding others wishing to undertake similar 3D DEM research. In extending the 2D slope to a 3D cone, the geometry of the Confederation Bridge was used a starting point.

SIMULATIONS

Overview of the DEM Model

The ice sheet is composed of rigid spherical ice particles of equal radius. At each timestep, the forces on each particle are calculated based on their contacting and bonded neighbours in order to explicitly update the position, velocity, and rotation of each particle at the next timestep.

The contact force between two contacting (overlapping) particles, P_i and P_j, is

$$F_{ij} = \underbrace{k_n \delta_{n_{ij}} - \gamma_n v_{n_{ij}}}_{normal\ component\ (F_n)} + \underbrace{k_t \delta_{t_{ij}} - \gamma_t v_{t_{ij}}}_{tangential\ component\ (F_t)}, \quad (1)$$

where F_{ij} is the force of P_i on P_j, k_n and k_t are coefficients of normal and tangential elasticity, γ_n and γ_t are coefficients of normal and tangential viscoelastic damping, $\delta_{n_{ij}}$ and $\delta_{t_{ij}}$ are the normal and tangential overlap[2] of P_i and P_j, and $v_{n_{ij}}$ and $v_{t_{ij}}$ are the normal and tangential velocities of P_i relative to P_j. Furthermore, F_t is truncated to ensure that $F_t \leq \mu F_n$, where μ is the coefficient of friction.[3] These contact forces are illustrated in Figure 1.

[1] Two dimensional models in which each particle represents an ice floe can also have interpretations in 3D, by assuming that ice floe thickness is constant or governed by a distribution.

[2] Whereas normal overlap is recalculated at each timestep from particle positions, tangential overlap is not a value that can be calculated for a single simulation timestep. The tangential overlap is a "historical" measure of the tangential displacement between the particles for the duration of contact.

[3] In particle collisions in which the tangential overlap, $\delta_{t_{ij}}$, far exceeds the normal overlap, $\delta_{n_{ij}}$, (e.g., two particles which closely skim each other) the forces calculated by equation (1) might result in tangential frictional forces which are disproportionately high in relation to normal elastic forces. Hence the need to truncate F_t.

The values of k_n, k_t, γ_n, and γ_t are calculated in LIGGGHTS from Young's modulus, Poisson's ratio, coefficient of restitution, particle diameter, particle mass, and normal overlap according to a Hertz-Mindlin derivation similar to that found in Pöschel and Schwager (2005). Because k_n, k_t, γ_n, and γ_t depend on normal overlap, they vary with each timestep.

Particle bonds are based on the parallel bond model described in Potyondy and Cundall (2004). In this model, a bond behaves like a set of parallel springs forming a cylindrical strut between the particles. The bonds resist tension, compression, shear, twisting, and bending as a function of normal and tangential bond stiffness. This behaviour is illustrated in Figure 2. Bonds are broken when the normal or tangential stress on the bond (σ and τ, respectively) exceed a specified strength. The values of σ and τ are calculated according to

$$\sigma = \frac{|F_n|}{\pi {R_b}^2} + \frac{4|T_t|}{\pi {R_b}^3}, \tag{2}$$

$$\tau = \frac{|F_t|}{\pi {R_b}^2} + \frac{2|T_n|}{\pi {R_b}^3}, \tag{3}$$

where T_t and T_n are the relative tangential and normal torque on the particles (i.e., "bend" and "twist") and R_b is the radius of the circular cross-section of the cylindrical bond strut.

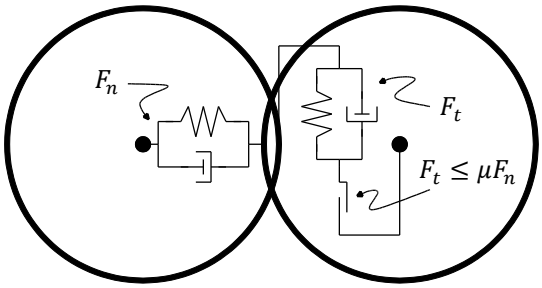

Figure 1: Contact forces (normal/tangential spring dashpots, tangential frictional slider).

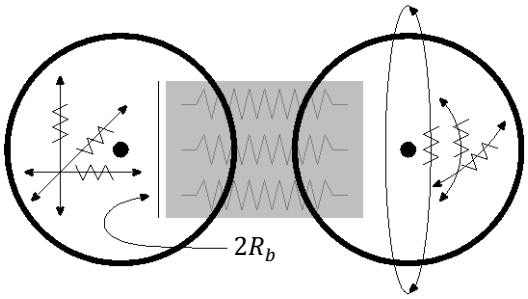

Figure 2: Parallel bonds resist tension, compression, shear, twisting, and bending.

The cone is composed of surface elements resulting from a meshing. Once LIGGGHTS determines that an ice particle has come in contact with a surface element, the same particle-particle contact calculations are used to resolve the particle-surface contact, where the surface element is represented as a particle with radius approaching infinity. Whether the particle collides with the surface on a facet, edge, or corner, the same stiffness and damping values are used, with normal forces being directed from the point of contact through the particle centre.

In this study, all adjacent particles in the ice sheet were bonded at the outset and bonds were not allowed to reform once they were broken (i.e., no refreezing); moreover, ice particles were not allowed to adfreeze to the cone. To represent a large ice sheet rubbling against the cone, the (finite-sized) ice sheet was bounded by walls on the sides, with the cone moving into the ice. Gravity, buoyancy, and water drag forces were also included in the simulations.

Simulation Parameters

The bulk of this investigation consists of 14 simulations (supported by many additional simulations which served to understand the effects of bond parameters and particle packings). The parameters for the simulations are given in Table 1 and Table 2.

Particles were packed into the ice sheet using a hexagonal close packing, which maximized the volume occupied by the particles relative to the inter-particle space. Early simulations which used a cubic packing led to flexure and force chains which tended to follow the orthogonality inherent in the packing, which was unrealistic. Because any packing of non-overlapping spheres to represent a non-spherical object (e.g., ice sheet) will result in a significant amount of empty space, either the density of the ice particles/water or the volume calculation associated with the ice particles must be adjusted in order to ensure that buoyancy is accurately modelled. For this study, the density value and volume calculations were not adjusted (i.e., $\rho_{ice} = 900$ kg·m^{-3}, $\rho_{water} = 1010$ kg·m^{-3}, from Paavilainen and Tuhkuri (2013)), recognizing that the modelled ice sheet will sit slightly lower in the water column.

To stabilize the buoyant particles, a drag force was added using a value of 0.00188 N·s·m^{-2} for the viscosity of sea water (Engineering Toolbox, 2014). No "added mass" effect was accounted for, as the speed of the ice sheet (cone) was reasonably slow (0.5 m·s^{-1}).

Given that the nature of the investigation is qualitative, reasonable parameter values for bulk ice sheets are reasonable values for the particles. Notably, a Young's modulus of 10^9 N·m^{-2} (i.e., 1 GPa)[4] and a Poisson's ratio of 0.3 were used for the ice particles, the latter value being taken from Paavilainen and Tuhkuri (2013). In turn, an upper bound for the timestep, $\bar{t}$, of 3.107×10^{-4} s was determined using the p-wave velocity, v_p, according to:

$$\bar{t} \leq \frac{d_{min}}{v_p} = d_{min}\left[\frac{E(1-\nu)}{(1+\nu)(1-2\nu)\rho_{ice}}\right]^{-\frac{1}{2}}, \tag{4}$$

where d_{min} is the diameter of the smallest particle. Based on this upper bound, a conservative timestep of 10^{-5} s was used in all simulations.

While an ice-ice coefficient of friction value of 0.1 was used by Paavilainen and Tuhkuri (2013) for their highly regular polygonal blocks, these simulations used a value of 0.3 as the spherical particles actually represent irregular surfaces which may be experiencing some crushing when they contact neighbouring blocks of rubble. For the same reason, the ice-cone coefficient of friction value of 0.3 was taken from the work of Paavilainen and Tuhkuri (2013), and a very low coefficient of restitution for ice-ice and ice-cone interactions was used (0.01). As was the case with the Young's modulus, detailed calibration to represent bulk effects was not considered.

The radius of the circular cross-section of the cylindrical particle bond strut, R_b, was set to the particle radius. The normal bond stiffness per unit area, $\bar{k}_n$, was derived according to

$$\bar{k}_n = \frac{k}{A_{bond}} = \frac{E}{l} = \frac{E}{d}. \tag{5}$$

The tangential bond stiffness per unit area, $\bar{k}_t$, was set to the same value.

The most challenging parameter values to set were those of the bonds strengths. The maximum normal and tangential bond strengths, σ_{max} and τ_{max}, were set to be equal at about 9×10^4 N·m^{-2} (i.e., 90 kPa). This value is such that the ratio of bond strength to particle stiffness ($\frac{\sigma_{max}}{E} = 9\times10^{-5}$), which largely governs flexural failure, is comparable to that of the ratios of flexural strength of an ice sheet (~5×10^5 N·m^{-2}) to its stiffness (~5×10^9 N·m^{-2}). For further discussion on these values, see Palmer and Croasdale (2013) and ISO 19906:2010.

[4] Early calibration testing associated with other research by one of the authors suggests a 1 to 3 ratio between particle stiffness and bulk stiffness.

In generating the cones, 12 facets were used to ensure a reasonably "curved" surface without increasing the computational complexity. Compared with 12-faceted cones, preliminary simulations using 64 facets showed little difference in rubble pile formation. Similarly, whether the ice sheet hit the cone at a leading edge (join of two facets), or hit it squarely on a facet, proved largely irrelevant: after a brief period, the shape of the rubble pile negated the effect of the profile of the cone. When the ice sheet hit the cone squarely on a facet, only very localized increases in rubble height were observed on the face (i.e., minor localized ride-up).

The cone angles used for the study were 52° and 30°.[5] The 52° cone, which also features an increased cone angle of 78° near the top, matches those found on the Confederation Bridge (see Brown et al. (2010)). For each cone, the depth below the waterline and the diameter at the waterline was constant. The ice speed of 0.5 $m \cdot s^{-1}$ was considered reasonable and within the range of values suggested in ISO 19906:2010 for several arctic locations.

In setting the size of the ice sheet, the intent was to reduce the boundary effects resulting from the immovable bounding walls without significantly increasing the number of particles. The simulations featuring a single layer of particles had about 18 m of extra ice on each side of the cone (i.e., distance from the edge of the cone to the bounding wall) and 50 m of extra ice on the far end, whereas the simulations featuring three layers of particles had about 13 m of extra ice on each side and 25 m of extra ice on the far end.

Table 1: Common simulation parameter values.

	Parameter		**Units**	**Value**
Particles	Young's modulus, E		$N \cdot m^{-2}$	10^9
	Poisson ratio, ν		-	0.3
	Density, ρ_{ice}		$kg \cdot m^{-3}$	900
	Coeff. of ice-ice friction		-	0.3
	Coeff. of ice-cone friction		-	0.3
	Coeff. of ice-ice restitution		-	0.01
	Coeff. of ice-cone restitution		-	0.01
	Packing		-	HCP
Water	Density, ρ_{water}		$kg \cdot m^{-3}$	1010
	Viscosity		$N \cdot s \cdot m^{-2}$	0.00188
Cone	Ice (cone) velocity		$m \cdot s^{-1}$	0.5
	Cone diameter at waterline		m	~14
	Depth of cone below waterline		m	4
	Height of cone above waterline	52/78°	m	11
		30°	m	7.48
Misc.	Timestep, $\bar{t}$		s	10^{-5}

[5] The 30° cone, which is unlikely to be seen in actual design due the increase in material cost, has been taken from the work of Paavilainen and Tuhkuri (2013). Though the 30° angle makes more sense in the 2D context (e.g., a shoreline) the 30° cone has been useful in the 3D context to understand the impact of an extreme design.

Table 2: Test matrix.

	Parameter	Units	Simulation													
			52	**53**	**54**	**55**	**56**	**57**	**61**	**62**	**63**	**64**	**65**	**66**	**70**	**71**
Ice sheet	Length	m	100	100	50	50	100	100	100	100	50	50	100	100	100	100
	Width	m	50	50	40	40	50	50	50	50	40	40	50	50	50	50
	Thickness, h	m	1	1	~1	~1	0.5	0.5	1	1	~1	~1	0.5	0.5	1	0.5
	# of layers of particles, w	-	1	1	3	3	1	1	1	1	3	3	1	1	1	1
Particles	Diameter, $d = \frac{h}{1+(w-1)\sqrt{2/3}}$	m	1	1	0.38	0.38	0.5	0.5	1	1	0.38	0.38	0.5	0.5	1	0.5
	Bond radius, $R_b = \frac{d}{2}$	m	No bonding	No bonding	No bonding	No bonding	No bonding	No bonding	0.5	0.5	0.19	0.19	0.25	0.25	0.5	0.25
	Normal bond stiffness per unit area, $\bar{k}_n = \frac{E}{d}$	N·m^{-3}							10^9	10^9	2.63×10^4	2.63×10^4	2×10^4	2×10^4	10^9	2×10^4
	Tang. bond stiffness per unit area, $\bar{k}_t = \bar{k}_n$	N·m^{-3}							10^9	10^9	2.63×10^4	2.63×10^4	2×10^4	2×10^4	10^9	2×10^4
	Max. normal bond stress, σ_{max}	N·m^{-2}							9×10^4	9×10^4	10^5	10^5	9×10^4	9×10^4	6×10^4	6×10^4
	Max. tangential bond stress, $\tau_{max} = \sigma_{max}$	N·m^{-2}							9×10^4	9×10^4	10^5	10^5	9×10^4	9×10^4	6×10^4	6×10^4
Misc.	Cone angle, α	degrees	52	30	52	30	52	30	52	30	52	30	52	30	30	30
	Time simulated, $t_{max} \cdot \bar{t}$	s	100	100	50	50	100	100	100	100	50	50	100	100	100	100

OBSERVATIONS

Impact of Bonds on Rubbling

For comparative purposes, three metrics were used to quantify the rubble pile: the height of the highest particle (${z_{max}}^t = \max\{z_p^t, p \in P\}$), the height (depth) of the lowest particle (${z_{min}}^t = \min\{z_p^t, p \in P\}$), and the summed deviation of the particles from the height of the highest particle at t = 0 (i.e., the floating level; $\Sigma(|\Delta z|)^t = \Sigma_{p \in P}|z_p^t - {z_{mx}}^0|$), where P is the set of all particles in the simulation, and z_p^t is the height of particle p at the current timestep t. Each metric is based on particle centres, thereby removing diameter from the calculation.

In the case of an ice sheet composed of a single layer of particles (w = 1), bonding had a significant impact on rubbling by making the rubble pile more extreme in height/depth. This impact is illustrated in Figure 3, Figure 4, and Figure 5 which compare z_{max}, z_{min}, and $\Sigma(|\Delta z|)$ values between non-bonded and bonded simulations using the same parameters. Notably, once a "steady-state" rubble pile developed, the height of the highest particle was 4 to 6 times higher in simulations using bonded particles. In the case of thicker ice, the earliest parts of the ice-cone interaction saw maximum heights greater than 10 times higher with bonded particles, and the lowest particles were about 1.5 to 2 times deeper in the "steady-state".

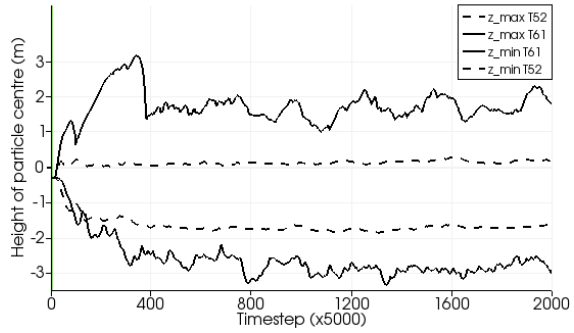

Figure 3: z_{max} and z_{min}, T52 and T61.

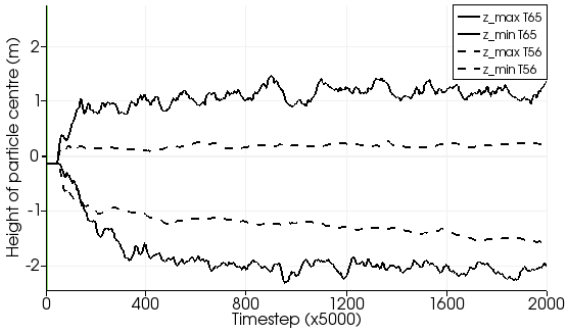

Figure 4: z_{max} and z_{min}, T56 and T65.

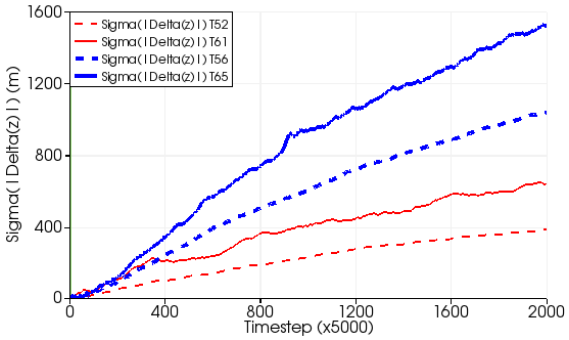

Figure 5: $\Sigma(|\Delta z|)$, T52, T61, T56, and T65.

In the case of a 3-layer sheet (w = 3), bonding caused the maximum height of the rubble pile to be 4 to 5 times higher, yet the minimum height (depth) was raised slightly (Figure 6); moreover, the values for $\Sigma(|\Delta z|)$ were nearly identical in the bonded and unbonded case (Figure 7). These results suggest that, for bonded particles, a significant increase in height of

a few particles at the top of the rubble pile was offset by a similar significant increase in the number of particles sitting closer to the waterline. Overall, bonding caused the rubble pile to ride higher and sit higher relative to the waterline.

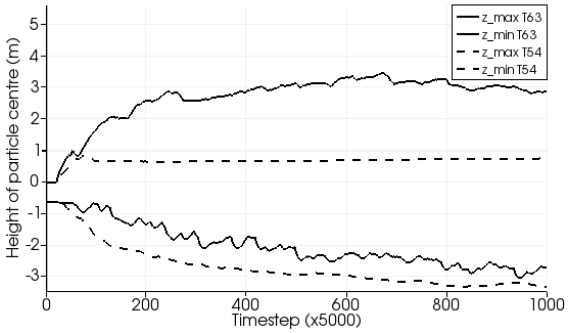

Figure 6: z_{max} and z_{min}, T54 and T63.

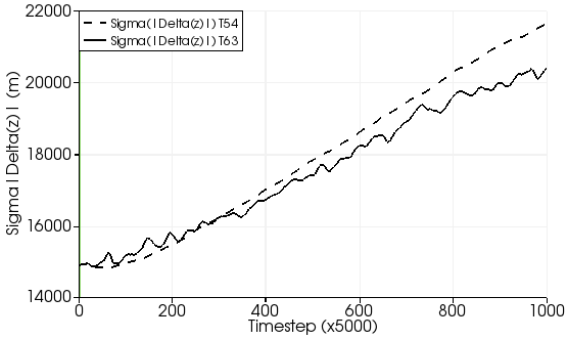

Figure 7: $\Sigma(|\Delta z|)$, T54 and T63.

Early simulations determined that σ_{max} and τ_{max} did not have a wide range with respect to effectively demonstrating flexural failure of the ice sheet. This sensitivity is illustrated in Figure 8 (flexural failure is realistic), Figure 9 (the ice is "weak"), and Figure 10 (the ice holds together, but is "springy).

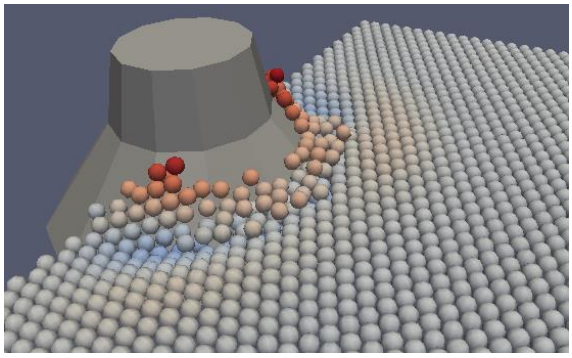

Figure 8: T61 ($\sigma_{max} = \tau_{max}$ = 9×10^4 N·m^{-2}, $h = d$ = 1m, α = 52°).

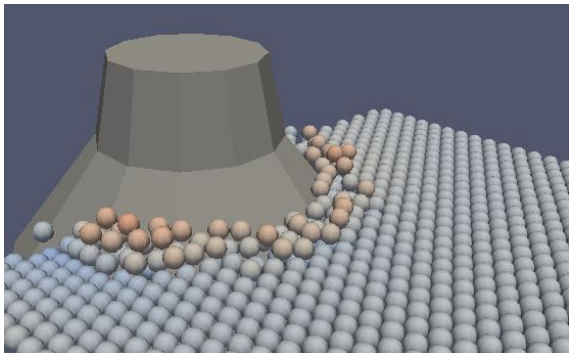

Figure 9: "Weak" ice in T40 (similar to T61, but $\sigma_{max} = \tau_{max}$ = 8×10^4 N·m^{-2}).

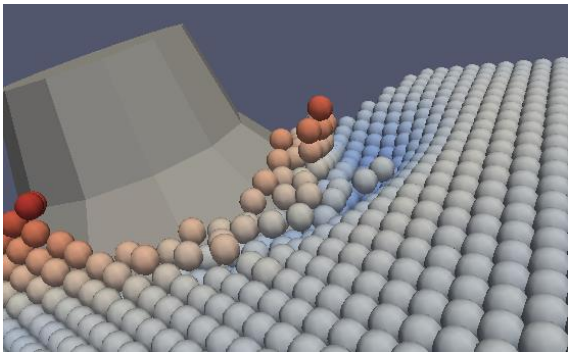

Figure 10: "Springy" ice in T47 (similar to T61, but $\sigma_{max} = \tau_{max}$ = 1×10^5 N·m^{-2}).

Very early simulations investigated the use of a simple bond breakage condition based upon displacement: if two bonded particles separated by more than a specified distance, the bond

would break. This displacement-based breakage condition, though simple to understand, meant that the torque on a particle did not contribute to bond fracture, which is unrealistic. Hence the breakage conditions of equations (2) and (3) were adopted.

Sheet Composition

The simulation which best reflected past observations at the Confederation Bridge presented in Brown et al. (2010) was T63 (see Figure 11) which used three layers (w = 3) to generate the 1m thick sheet. Generally, the use of multiple layers with the hexagonal close packing allowed irregular slabs of ice to flex, break, rotate, and slide. Some blocks "tumbled" and broke into smaller blocks. In some cases, local fracturing occurred as individual particles chipped off the sides. Figure 11 shows a large intact slab of ice sitting on the top of the rubble pile and Figure 12 shows intact slabs of ice on the interface between the rubble pile and the cone (viewed from the perspective of the cone, which has been removed).

The use of multiple layers of particles to form the ice sheet led to greater realism; however, this also led to much slower simulations as the number of particles in a sheet of fixed size grows according to $\theta(w^3)$, where w is the number of layers used to construct the sheet. Notably, T61, which simulated a 100m×50m×1m 1-layer sheet composed of 5729 particles interacting for 100s, took 77171s to run on one processor, whereas T63, simulating a 50m×40m×1m 3-layer sheet composed of 48048 particles interacting for 50s, took 868487s to run on two processors.

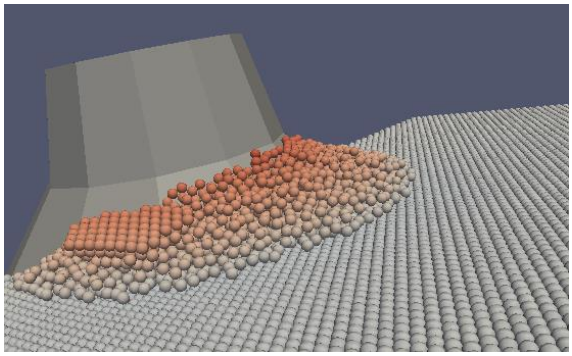

Figure 11: T63 (w = 3), t = 1500000.

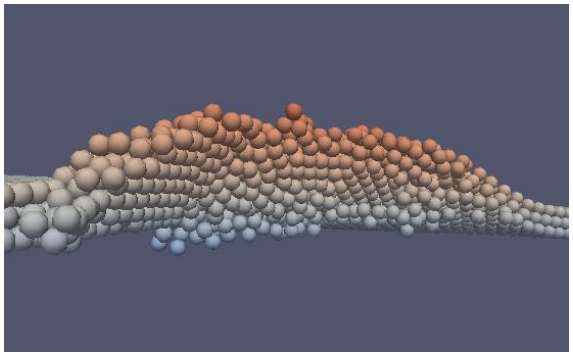

Figure 12: T63 (w = 3), t = 650000, cone removed.

Sheet Thickness

The comparisons of T61 and T65 that can be made using Figure 8 and Figure 13 illustrate the differences in the rubble pile between a 1m thick sheet (h = 1m) and a 0.5m thick sheet (h = 0.5m). The ice in the thicker sheet broke into larger slabs which rode higher and were forced deeper, whereas the thinner sheet mostly broke into individual particles.

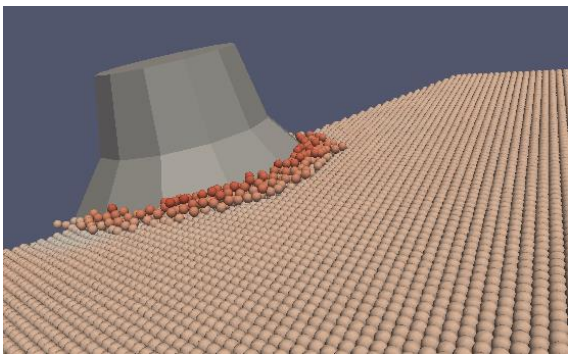

Figure 13: T65 (α = 52°, $h = d$ = 0.5 m), t = 1625000.

CONCLUSIONS AND FUTURE WORK

This work uses a three-dimensional discrete element method (3D DEM) bonded particle model to simulate ice interaction with an upward-sloping cone to observe rubble pile formation and clearance around the sides. In contrast with past 2D investigations of ice interactions with slopes, which use finite element methods (FEM) to determine ice sheet fracture, this investigation realizes fracture solely using DEM.

Generally, the simulations demonstrated key ice-cone interaction processes, such as flexural failure and rubble pile ride-up, rotation, and collapse. With respect to the impact of ice thickness on rubbling, results are consistent with past 2D DEM work of Paavilainen and Tuhkuri (2012): thicker ice leads to a rubble pile of greater height and depth.

The use of multiple layers of particles to form the ice sheet led to greater realism; however, this also led to much slower simulations. Future convergence testing could identify the optimal number of layers which effectively balances computation time with accuracy.

The values for normal and tangential particle bond strength which best showed the failure of the ice in flexure did not have a wide range. Future extensions of this research should tailor these bonding parameters (including unequal normal and tangential components) to more accurately represent the flexural strength of ice, and implement bond visualization to better visualize the fracture process.

Improved representation of ice properties through the development of models that better capture particle contacts, bonding, ice defects, and strength variations, will enable the 3D DEM simulations performed in this study to be enhanced. Notably, ridges can be added, rubble can be allowed to refreeze, and material parameters can be calibrated to allow measurement of forces. Further numerical experiments building off those presented in this work will allow us to better understand the complex interaction of ice against sloping structures for a range of ice conditions.

ACKNOWLEDGEMENTS

The authors gratefully acknowledge core funding for the C-CORE Centre for Arctic Resource Development (CARD) by the Hibernia Management and Development Company (HMDC), the Terra Nova project, and the Research and Development Corporation of Newfoundland and Labrador (RDC). As well, the authors would like to thank the many members of C-CORE and CARD who provided helpful suggestions and comments in support of this research.

REFERENCES

Brown, T.G., Tibbo, J.S., Tripathi, D., Obert, K. and Shrestha, N., 2010. Extreme ice load events on the Confederation Bridge. *Cold Regions Science and Technology*, 60(2010), pp. 1-14.

Cundall, P.A., 1971. A computer model for simulating progressive large scale movements in blocky rock systems. In: International Society for Rock Mechanics (ISRM), *Proceedings of the International Symposium on Rock Fracture: Volume 1*. Nancy, France.

Engineering Toolbox, 2014. *Sea Water Properties*. [online] Available at http://www.engineeringtoolbox.com/sea-water-properties-d_840.html [Accessed November 30, 2014].

Hasse, A., Polojärvi, A. and Tuhkuri, J., 2010. 3D discrete numerical modelling of a conical structure-ice rubble interaction. In: International Association for Hydro-Environment Engineering and Research (IAHR), *Proceedings of the 20th IAHR International Symposium on Ice (IAHR ICE 2010)*. Lahti, Finland, 14-18 June 2010.

Hopkins, M.A. and Hibler III, W.D., 1991(a). On the shear strength of geophysical scale ice rubble. *Cold Regions Science and Technology*, 19(1991), pp. 201-212.

Hopkins, M.A. and Hibler III, W.D., 1991(b). On the ridging of a thin sheet of lead ice. *Annals of Glaciology*, 15(1991), pp. 81-86.

Hopkins, M.A., Hibler III, W.D. and Flato, G.M., 1991. On the numerical simulation of the sea ice ridging process. *Journal of Geophysical Research*, 96(C3), pp. 4809-4820.

International Organization for Standardization, 2010. ISO 19906:2010 *Petroleum and natural gas industries – Artic offshore structures*. Geneva, Switzerland.

Kioka, S., Yamamoto, Y., Sugawara, K., Endo, T. and Takeuchi, T., 2010. Medium-scale experiment and numerical simulations using 3-D DEM for the impact load by an ice floe against a pile structure. In: International Association for Hydro-Environment Engineering and Research (IAHR), *Proceedings of the 20th IAHR International Symposium on Ice (IAHR ICE 2010)*. Lahti, Finland, 14-18 June 2010.

Kloss, C., Goniva, C., Hager, A., Amberger, S. and Pirker, S., 2012. Models, algorithms and validation for opensource DEM and CFD-DEM. *Progress in Computational Fluid Dynamics, An International Journal*, 12(2/3), pp. 140-152.

Lu, W., Lubbad, R., Høyland, K. and Løset, S., 2014. Physical model and theoretical model study of level ice and wide sloping structure interactions. *Cold Regions Science and Technology*, 101(2014), pp. 40-72.

Lubbad, R. and Løset, S., 2011. A numerical model for real-time simulation of ship-ice interaction. *Cold Regions Science and Technology*, 65(2011), pp. 111-127.

Metrikin, I. and Løset, S., 2013. Nonsmooth 3D discrete element simulation of a drillship in discontinuous ice. In: *Proceedings of the 22nd International Conference on Port and Ocean Engineering under Arctic Conditions (POAC 2013)*. Espoo, Finland, 9-13 June 2013.

Metrikin, I., Borzov, A., Lubbad, R. and Løset, S., 2012(a). Numerical simulation of a floater in a broken-ice field – Part II: comparative study of physics engines. In: American Society of Mechanical Engineers (ASME), *Proceedings of the 31st International Conference on Ocean, Offshore and Arctic Engineering (OMAE 2012)*. Rio de Janeiro, Brazil, 1-6 July 2012.

Metrikin, I., Lu, W., Lubbad, R., Løset, S. and Kashafutdinov, M., 2012(b). Numerical simulation of a floater in a broken-ice field – Part I: model description. In: American Society of Mechanical Engineers (ASME), *Proceedings of the 31st International Conference on Ocean, Offshore and Arctic Engineering (OMAE 2012)*. Rio de Janeiro, Brazil, 1-6 July 2012.

Paavilainen, J. and Tuhkuri, J., 2012. Parameter effects on simulated ice rubbling forces on a wide sloping structure. *Cold Regions Science and Technology*, 81(2012), pp. 1-10.

Paavilainen, J. and Tuhkuri, J., 2013. Pressure distributions and force chains during simulated ice rubbling against sloped structures. *Cold Regions Science and Technology*, 85(2013), pp. 157-174.

Palmer, A. and Croasdale, K., 2013. *Arctic Offshore Engineering*, Hackensack, USA: World Scientific.

Polojärvi, A. and Tuhkuri, J., 2009. 3D discrete numerical modelling of ridge keel punch through tests. *Cold Regions Science and Technology*, 56(2009), pp. 18-29.

Polojärvi, A. and Tuhkuri, J., 2013. On modelling cohesive ridge keel punch through tests with a combined finite-discrete element method. *Cold Regions Science and Technology*, 85(2013), pp. 191-205.

Polojärvi, A. and Tuhkuri, J., 2014. 3D DEM for freeze bonded ice rubble consisting of polyhedral blocks. In: International Association for Hydro-Environment Engineering and Research (IAHR), *Proceedings of the 22nd IAHR International Symposium on Ice (IAHR ICE 2014)*. Singapore, 11-15 August 2014.

Polojärvi, A., Tuhkuri, J. and Korkalo, O., 2012. Comparison and analysis of experimental and virtual laboratory scale punch through tests. *Cold Regions Science and Technology*, 81(2012), pp. 11-25.

Pöschel, T. and Schwager, T., 2005. *Computational Granular Dynamics: models and algorithms*. Berlin: Springer-Verlag.

Potoyondy, D.O. and Cundall, P.A., 2004. A bonded-particle model for rock. *International Journal of Rock Mechanics and Mining Sciences*, 41(8), pp. 1329-1364.

Richard, M. and McKenna, R., 2013. Factors influencing managed sea ice loads. In: *Proceedings of the 22nd International Conference on Port and Ocean Engineering under Arctic Conditions (POAC 2013)*. Espoo, Finland, 9-13 June 2013.

Sorsimo, A. and Heinonen, J., 2014. Modelling ice ridge punch test with cohesive 3D discrete element method. In: International Association for Hydro-Environment Engineering and Research (IAHR), *Proceedings of the 22nd IAHR International Symposium on Ice (IAHR ICE 2014)*. Singapore, 11-15 August 2014.

Vroegrijk, E.A.J., 2012. Application of the discrete element method on ship-ice interaction. In: Society of Naval Architects and Marine Engineers (SNAME), *Proceedings of the 10th International Conference and Exhibition on Ships and Structures in Ice (ICETECH 2012)*. Banff, Canada, 17-20 September 2012.